Development of an Automated Method for the Detection of Chronic Lacunar Infarct Regions in Brain MR Images

Article *in* IEICE Transactions on Information and Systems · June 2007

DOI: 10.1093/ietisy/e90-d.6.943 · Source: OAI

12 authors, including:

Xuejun Zhang
Guangxi University
99 PUBLICATIONS **352** CITATIONS
SEE PROFILE

Hiroshi Fujita
Gifu University
551 PUBLICATIONS **6,173** CITATIONS
SEE PROFILE

Takeshi Hara
Gifu University
282 PUBLICATIONS **3,042** CITATIONS
SEE PROFILE

Xiangrong Zhou
Gifu University
131 PUBLICATIONS **1,404** CITATIONS
SEE PROFILE

PAPER

Development of an Automated Method for the Detection of Chronic Lacunar Infarct Regions in Brain MR Images

Ryujiro YOKOYAMA[†a)], **Xuejun ZHANG**[†,††††], ***Nonmembers***, **Yoshikazu UCHIYAMA**[†], **Hiroshi FUJITA**[†], **Takeshi HARA**[†], **Xiangrong ZHOU**[†], ***Members***, **Masayuki KANEMATSU**[††], **Takahiko ASANO**[††], **Hiroshi KONDO**[††], **Satoshi GOSHIMA**[††], **Hiroaki HOSHI**[††], ***and*** **Toru IWAMA**[†††], ***Nonmembers***

SUMMARY The purpose of our study is to develop an algorithm that would enable the automated detection of lacunar infarct on T1- and T2-weighted magnetic resonance (MR) images. Automated identification of the lacunar infarct regions is not only useful in assisting radiologists to detect lacunar infarcts as a computer-aided detection (CAD) system but is also beneficial in preventing the occurrence of cerebral apoplexy in high-risk patients. The lacunar infarct regions are classified into the following two types for detection: "isolated lacunar infarct regions" and "lacunar infarct regions adjacent to hyperintensive structures." The detection of isolated lacunar infarct regions was based on the multiple-phase binarization (MPB) method. Moreover, to detect lacunar infarct regions adjacent to hyperintensive structures, we used a morphological opening processing and a subtraction technique between images produced using two types of circular structuring elements. Thereafter, candidate regions were selected based on three features — area, circularity, and gravity center. Two methods were applied to the detected candidates for eliminating false positives (FPs). The first method involved eliminating FPs that occurred along the periphery of the brain using the region-growing technique. The second method, the multi-circular regions difference method (MCRDM), was based on the comparison between the mean pixel values in a series of double circles on a T1-weighted image. A training dataset comprising 20 lacunar infarct cases was used to adjust the parameters. In addition, 673 MR images from 80 cases were used for testing the performance of our method; the sensitivity and specificity were 90.1% and 30.0% with 1.7 FPs per image, respectively. The results indicated that our CAD system for the automatic detection of lacunar infarct on MR images was effective.

key words: *brain MRI, lacunar infarct, computer-aided diagnosis, T1- and T2-weighted images, mathematical morphology*

1. Introduction

The use of magnetic resonance imaging (MRI) has spread rapidly over the last 10 years. As a result, MRI of the brain has been widely used in many hospitals to detect intracranial arterial aneurysms and to decrease the incidence of subarachnoid hemorrhage. For example, "brain dock," also brain check-up, is an inspection method used for detecting asymptomatic brain diseases by using MRI- and magnetic resonance angiography (MRA)-based image diagnosis. This helps neuroradiologists and/or neurosurgeons to detect the factors that give rise to brain diseases and to prevent the possible emergence of a disease. Recently, the application of brain dock has been extended to detect asymptomatic cerebral infarction and leukoaraiosis in their early stages in order to advise patients regarding their life-style changes that reduce the risk of brain diseases and to prevent the occurrence of serious cerebral infarction [1].

Asymptomatic cerebral infarction (also referred to as lacunar infarct) was defined by Fisher as a disease with special lacunar symptom caused by the occlusion of a single penetrating artery and was regarded as the most dangerous consequence of hypertension [2]. Most lacunar infarcts are small in size (< 10 mm) and are located in the region of the penetrating branch; they often occur in the upper two-thirds of the basal ganglia [3]. MRI of lacunar infarcts appears heterogeneous and irregular in shape with diameters of approximately 3 to 10 mm. The intensity of lacunar infarcts appears low in T1-weighted images but high in T2-weighted images [4]. While acute lacunar infarct can be detected in the diffusion weighted image (DWI) easily, subacute or chronic ones are hard to identify in the DWI. Therefore, we focused on the chronic ones in this study.

Lacunar infarct is believed to be strongly related to cerebral apoplexy in patients with hypertension. If a lacunar infarct region is detected by MRI using a high-intensity signal, the existing hypertension will increase the possibility of future cerebral apoplexy by 10 times [5]. Therefore, computer-aided detection (CAD) of lacunar infarct regions may help neuroradiologists and/or neurosurgeons to interpret a large number of images, diagnose high-risk cerebral apoplexy patients, and possibly prevent severe cerebral apoplexy by proper management of risk factors through blood investigations and life-style changes. In this study, we developed an algorithm that enabled a fully automatic detection of lacunar infarcts in T2-weighted MR images as a part of our CAD system for the brain.

Some studies have reported on the application of CAD by using MRI, such as the segmentation of tissues in brain MR imaging [6]–[9], the extraction of vessels in brain MRA [10], [11], and the detection of aneurysms in MRA [12]–[17]. However, there have been no reports on the use of CAD in the detection of lacunar infarcts with the exception of our recent initial basic research [18].

In contrast to our previous study on the automatic

Manuscript received June 20, 2006.
Manuscript revised January 11, 2007.

[†]The authors are with the Department of Intelligent Image Information, Graduate School of Medicine, Gifu University, Gifu-shi, 501–1194 Japan.
[††]The authors are with the Department of Radiology, Graduate School of Medicine, Gifu University, Gifu-shi, 501–1194 Japan.
[†††]The author is with the Department of Neurosurgery, Graduate School of Medicine, Gifu University, Gifu-shi, 501–1194 Japan.
[††††]The author is with the College of Computer Science and Information Engineering, Guangxi University, 100 Daxue Road, Nanning City, Guangxi 530004, P. R. China.
a) E-mail: ryujiro@fjt.info.gifu-u.ac.jp
DOI: 10.1093/ietisy/e90–d.6.943

detection of lacunar infarct regions, the new proposed method reported in this study uses multiple thresholds instead of a fixed threshold. Furthermore, for the elimination of false positives (FPs), the T1-weighted MR image was introduced to improve performance.

The developed method is described in detail in Sect. 2, and Sect. 3 describes the result of the experiment. The discussion is included in Sect. 4, followed by the conclusion in Sect. 5.

2. Materials and Methods

2.1 Clinical Cases

One hundred patients underwent MR imaging that employed a 1.5-T superconducting magnet (Signa Horizon; GE Medical Systems, Milwaukee, Wis.). The T2-weighted axial images were obtained by the fast spin-echo method using a quadrature head coil with the following settings: effective echo time (TE), 96–105 ms; repetition time (TR), 3000–3500 ms; echo train length (ETL), 5–14; number of excitations (NEX), repeated twice or thrice; slice thickness, 5 mm; slice gap, 2 mm; frequency encode step × phase encode step, 512×224 and 512×256; field of view (FOV), 240 mm. The T1-weighted axial images were obtained by the spin-echo method with the following settings: spin-echo TE, 8–10 ms; TR, 300–466.7 ms; NEX, repeated twice; slice thickness, 5 mm; slice gap, 2 mm; frequency encode step × phase encode step, 512 × 224; FOV, 240 mm. The sectional images in all cases were scanned parallel to the orbito-meatal line (OM line).

2.2 Overall Scheme for the Detection of Lacunar Infarcts

The overall flowchart of our computerized detection scheme is illustrated in Fig. 1. First, the candidates with lacunar infarcts are identified using T2-weighted images (Part A described in Sect. 2.3). Next, FPs are eliminated by using T1-weighted images (Part B described in Sect. 2.4). Finally, the residual candidate regions are confirmed as being the lacunar infarct regions. We describe our method in detail in the following order, as illustrated in Fig. 1.

2.3 Detection of Lacunar Infarct Candidates Using the T2-Weighted Image (Part A)

Based on the location of lacunar infarct in the image, the lacunar infarct regions are classified into two types: isolated lacunar infarct regions and lacunar infarct regions adjacent to hyperintensive structures [Fig. 12, panel (a)]. If we apply only the binarization process to these two types of lacunar infarct regions, the candidates are then extracted together with the other hyperintensive tissues. Thus, it is difficult to accurately calculate the features such as area, circularity, and gravity center of candidates. Therefore, it is essential to use different methods for the detection of these two types

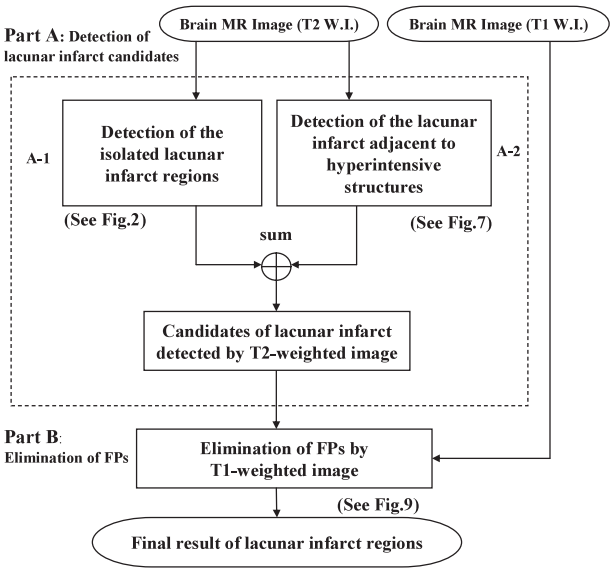

Fig. 1 The overall flowchart of our computerized detection scheme.

of lacunar infarct regions, particularly the lacunar infarct regions adjacent to the hyperintensive tissues. To overcome this issue, the mean pixel value of the cerebral ventricle was used as the reference threshold for the detection of the isolated lacunar infarct regions (A-1), and the candidates were detected using multiple threshold values for the binarization process—the MPB method. On the other hand, for the detection of lacunar infarct regions adjacent to the hyperintensive tissues (A-2), we used a morphological opening. The final lacunar infarct candidates are the sum of candidates detected by these two different methods.

2.3.1 Detection of the Isolated Lacunar Infarct Regions (A-1)

Generally, cerebral infarction is classified as acute, subacute, and chronic phases. The pixel values on MRI change according to the different phases of disease [19]. From acute to chronic phase, the abnormalities are liquefied, resulting in a prolonged T2 release time on MRI. Thus, the signal in the T2-weighted image becomes stronger, and the pixel values in the cerebral infarction region increase until an equilibrium value is reached at the chronic phase; this signal has the same intensity as that for the cerebrospinal fluid (CSF). This finding is the same as that observed in lacunar infarct disease, wherein the pixel values increase in definite steps from acute to chronic phase. Therefore, in this study, we propose the MPB method that uses several threshold values based on the mean pixel value of the cerebral ventricle as a reference threshold for the binarization of lacunar infarcts at acute, sub-acute, and chronic phases.

Figure 2 illustrates the flowchart for detecting the isolated lacunar infarct regions (A-1). First, the images are preprocessed as in (a)–(c). The extracted cerebral ventricle regions in (a) is used for determining a reference threshold in the MPB method. The extracted cerebral region in (b) is

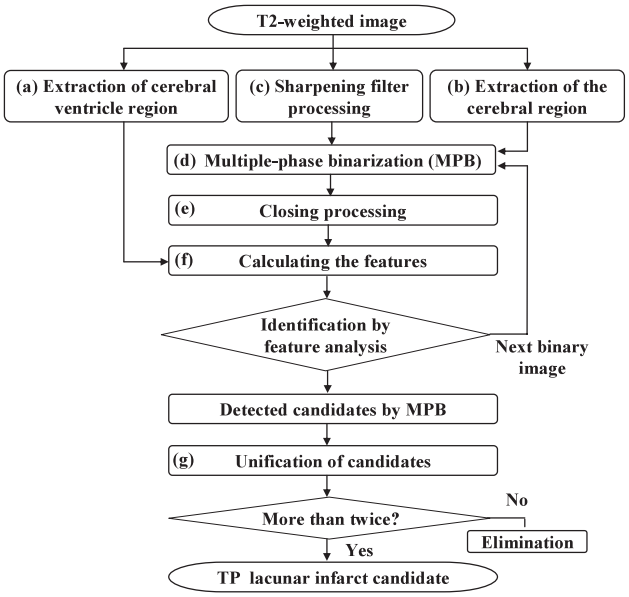

Fig. 2 Flowchart for detecting the isolated lacunar infarct regions (A-1).

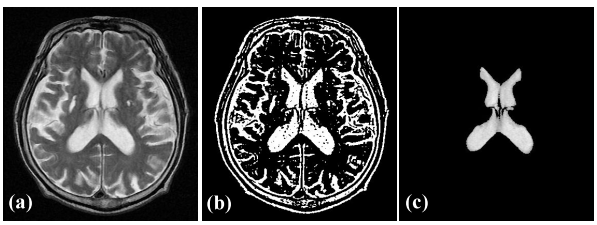

Fig. 3 Extraction of cerebral ventricle region. (a) Original T2-weighted image. (b) Binarized image. (c) Extracted cerebral ventricle region.

used for eliminating candidates outside this regions as FPs. The candidates of lacunar infarct were detected as shown in (d)–(g).

(a) Extraction of cerebral ventricle region: In order to calculate the mean pixel value in the cerebral ventricle region, which was used as the reference threshold for the MPB method, the cerebral ventricle (or cerebral sulci in its absence) region was segmented. The 7×7 Laplacian-type filter [18] was first used for the enhancement of the edges in the T2-weighted image. Subsequently, the cerebral ventricle region was extracted by simple binarization processing and feature analysis with size and location. Examples of images for the extraction of the cerebral ventricle region are illustrated in Fig. 3. In this figure, (a) is an original T2-weighted image, and (b) and (c) indicate the binarized image and the extracted cerebral ventricle region, respectively.

(b) Extraction of the cerebral region: Lacunar infarct is defined as a lesion that is mainly present in the basal ganglia region and in deep white matter. Therefore, the detection area can be limited to a circular area including these regions. In order to determine a circular area, the coordinates of the center point are required. We calculated the positions X_1, X_2, Y_1, and Y_2 corresponding to the left, right, top, and bottom positions of the cerebral regions, respectively, as shown

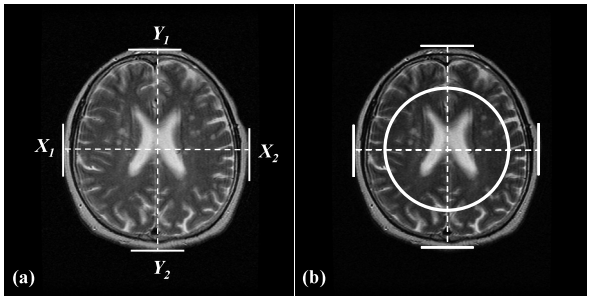

Fig. 4 Determination of a circular area for the detection of lacunar infarcts. (a) The center point of circular area. (b) The determined circular area. The candidates outside the circular area are considered as FPs.

in Fig. 4. These positions were obtained by the use of a simple threshold because the pixel values between the skin and background were considerably different. The intersection of the lines from X_1 to X_2 and Y_1 to Y_2 was defined as the center point of the circular area. The diameter of the circle was 70% of the length of X_1 and X_2. The fraction 70% was determined empirically by taking into account the size of basal ganglia region in the training dataset. Although this technique was very simple, all lacunar infarcts in the test dataset located within the circular area. Therefore, false negative cases were not occurred in our dataset. However, because the brain shape has certain variation, it may be necessary to modify this method in applying the large dataset in the future study.

(c) Sharpening filter processing: The median filter (3×3) and the unsharp mask filter were applied to the T2-weighted images for increasing the edge effect of lacunar infarct in order to improve the accuracy of detection and limit the number of FPs. In our experiment, the mask of the unsharp filter was set to 3×3 with $+8$ in the center element and -1 in the surrounding eight elements.

(d) Multi-phase binarization (MPB): We first calculated the mean pixel value of the extracted cerebral ventricle region. The reference threshold was then set to 70% of the mean pixel value. The thresholds for the MPB method were determined by increasing the pixel values in intervals of 5 pixel values from -45 to $+25$ pixel values of the reference threshold. Therefore, the total number of threshold values for the MPB processing included 15 phases.

(e) Closing processing: In order to delete the caves and holes in the binary images derived from 15 phases of MPB method, a closing processing is performed. This procedure has the effect of smoothing an object from outside to inside and allows the accurate calculation of the features.

(f) Calculation of the features: The following three features were calculated for the regions in each binary image.

[1] Area (A): number of pixels on a candidate.
[2] Circularity (C): defines the perimeter of a candidate l, then

$$C = 4\pi \times A/l^2. \tag{1}$$

[3] Gravity center $\{(g_x, g_y)\}$: mean value of the pixels

(x_i, y_i) in a candidate,

$$(g_x, g_y) = \left(\sum_{i=0}^{n-1} x_i/n, \sum_{i=0}^{n-1} y_i/n \right). \quad (i = 0, 1, 2, \cdots, n-1) \tag{2}$$

If the calculated features satisfy rules (3)–(5) given below, the region is considered as a candidate of lacunar infarct.

$$19 \leq A \leq 200 \tag{3}$$

$$0.45 \leq C \tag{4}$$

$$(g_x - c_x)^2 + (g_y - c_y)^2 < 12000, \tag{5}$$

where (c_x, c_y) is the center coordinate of an image derived in Sect. 2.3.1 (b). The area of lacunar infarct according to its diagnosis definition [3] ranged from approximately 3×3 mm to 10 × 10 mm. In case of our experiment, the size of one pixel was approximately 0.5 × 0.5 mm^2 (240/512), which was calculated from the FOV and the number of matrices. For example, a circular lacunar infarct of the smallest size, i.e., 3 mm in diameter, appeared on an area of approximately 7/0.25 = 28 pixels. Similarly, the lacunar infarct of the largest size, i.e., 10 mm in diameter, had a maximum area of approximately 79/0.25 = 316 pixels. We determined the threshold value of the area empirically based on the distribution of the lacunar infarcts in the 20 training data; the final range was set from 19 to 200 pixels. With regard to the 20 training data, all the candidates with an area from 5 to 400 pixels and with circularity from 0.30 to 1.0 were extracted and plotted on a graph (Fig. 5). When the threshold values are determined by using maximum and minimum values of the lacunar infarcts in the training dataset, the threshold values may strongly depend on the lacunar infarcts in the training dataset. Therefore, the threshold values represented by broken lines were selected so as to improve the stability and reliability of the threshold values by taking into account the size of clinical lacunar infarcts.

(g) Determination of candidates by their gravity centers: All the candidates detected by the MPB method were summed from their gravity centers (g_x, g_y). If a candidate center appears twice or more within a 3-pixel radius region $(g_x - 3 - g_x + 3, g_y - 3 - g_y + 3)$ away from the gravity center of a candidate, which is defined as the reference region, then that candidate was regarded as a TP of lacunar infarct. On the other hand, if it appears only once, it was considered as FP and was eliminated. A new position of gravity center is located from the centers of candidates. Among the detected candidates, if other gravity centers were present in the reference region, they were regarded as the same lacunar infarct with gravity centers that shifted only during the 15-phased MPB. All such gravity centers were integrated into one new center at the central point of each gravity center of the candidates. Four examples of the detected images obtained by the 15-phased MPB method are shown in Fig. 6.

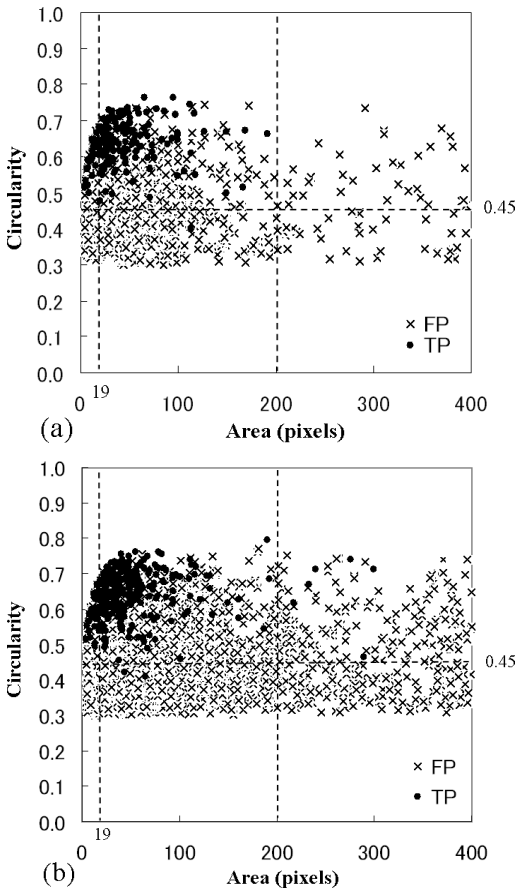

Fig. 5 Relationship between the area and circularity after the MPB method. (a) Training data (20 cases). (b) Testing data (80 cases). The threshold values are indicated by broken lines.

2.3.2 Detection of the Lacunar Infarct Adjacent to Hyperintensive Structures (A-2)

It is difficult to detect the lacunar infarct adjacent to the hyperintensive region because the region of lacunar infarct cannot be extracted using simple binarization. In order to detect these regions, morphological opening techniques defined by the two types of circular structuring elements with different radii were employed. The difference between the two images obtained by these techniques was used to detect the lacunar infarcts. Figure 7 shows the flowchart for detecting the lacunar infarcts adjacent to hyperintensive structures (A-2 in Fig. 1). These steps are described below in detail.

(a) Detection of TP candidates by morphological opening processing: The morphological opening processing is carried out by dilation processing following erosion processing. Using this method, the convex and small isolated regions in an image can be eliminated, and the smoothing effect can be concurrently achieved. In our method, circular structuring elements of different sizes were used, and the convex or small dot areas were detected on the resulting differential images. The kernels included two types of circles with radii of 1 and 8 pixels. The lacunar infarct regions

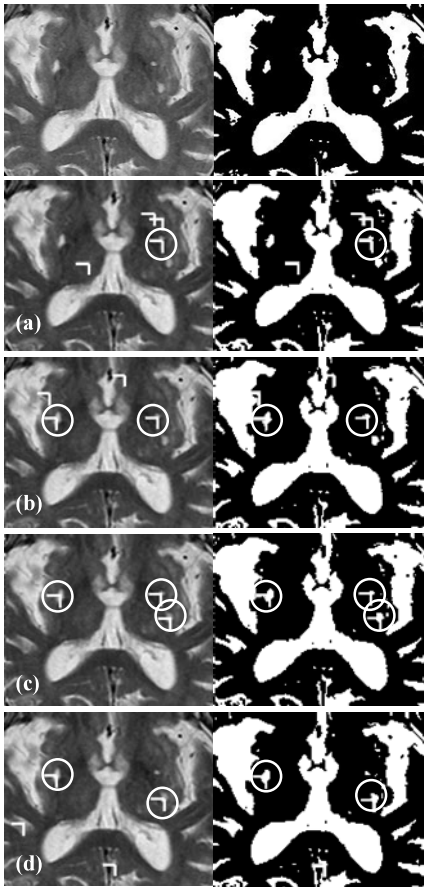

Fig. 6 Four examples of images of detection results obtained by the 15-phased MPB method. The white circles indicate lacunar infarcts. Top raw indicates original images. The threshold values of (a), (b), (c), and (d) are −40, −25, −10, and +5 pixel values from the reference threshold, respectively.

adjacent to the cerebral ventricles were discriminated using morphological opening processing and subtraction between the images reconstructed with two types of configuration elements. Thereafter, shrinking and binarization were employed to determine the final lacunar infarct regions according to the definition of area and circularity features described in Sect. 2.3.1 (f). The thresholds for area and circularity were $35 \leq A \leq 100$ and $0.35 \leq C$, respectively.

(b) Determination of TP candidates by using the region-growing method: The extracted candidates of lacunar infarct obtained by morphological opening processing and subtraction of images shown in (a) were almost circular or elliptical in shape. However, on analysis of the lacunar infarct regions adjacent to the cerebral ventricles, we noticed that there were subtle differences between the pixel values of lacunar infarct and CSF in the cerebral ventricles. This was the case even if a part of the lacunar infarct existed in the cerebral ventricles. Therefore, if the start-growing-point is set to the edge of an extracted candidate of the lacunar infarct region, then we can extract the lacunar infarct individually from the adjacent areas. Therefore, it was considered that these FPs could be easily eliminated by the area and

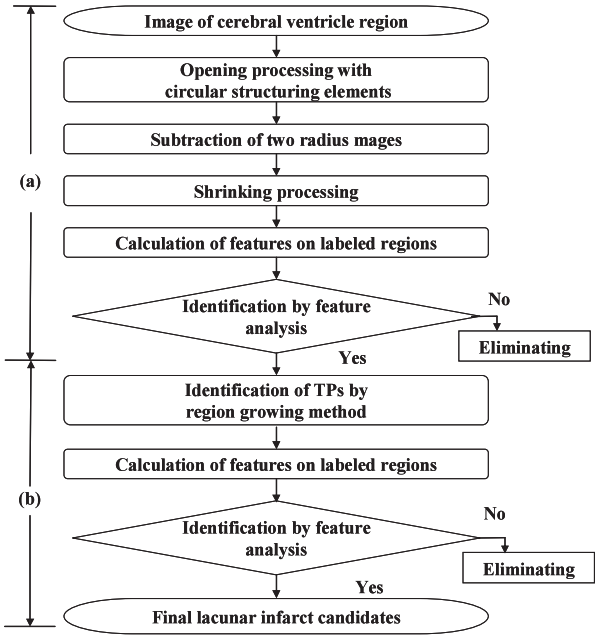

Fig. 7 Flowchart for detecting the lacunar infarcts adjacent to hyperintensive structures. (a) Procedure for the detection of TP candidates by morphological opening processing. (b) Determination of TP candidates by using the region growing method.

circularity features. The growing conditions were set using formulas (6) and (7).

$$Diff > |R_i - r_i|, \tag{6}$$

$$Min\_range < r_i < Max\_range, \tag{7}$$

where R_i is the gray level of the growing original pixel; r_i, gray level of the growing candidate pixel; $Diff$, difference between R_i and r_i; Max_range, maximum range; and Min_range, minimum range. The values of different parameters of the region growing, i.e., $range(Min\_range, Max\_range)$ and difference ($Diff$) are as follows: Min_range = mean value of the cerebral ventricle region × 0.5, $Max\_range = 255$, and $Diff = 3$. The thresholds of area and circularity are $25 \leq A \leq 100$ and $0.48 \leq C$, respectively.

In order to calculate the threshold value of area and circularity, all the candidates with area from 10 to 150 pixels and circularity from 0.30 to 1.0 were extracted from the 20 training data and plotted on a graph (Fig. 8). The threshold values were selected empirically so as to achieve a minimum number of FPs while keeping most of TPs in the training dataset.

2.4 Elimination of FPs by T1-Weighted Images (Part B)

A T1-weighted image is used to eliminate FPs from the candidates of lacunar infarct that were detected by the method described in part A. According to the definition stated in Sect. 1, lacunar infarcts appear as low-intensity signal areas in T1-weighted images and high-intensity signal areas in T2-weighted images. Therefore, the detected lacunar

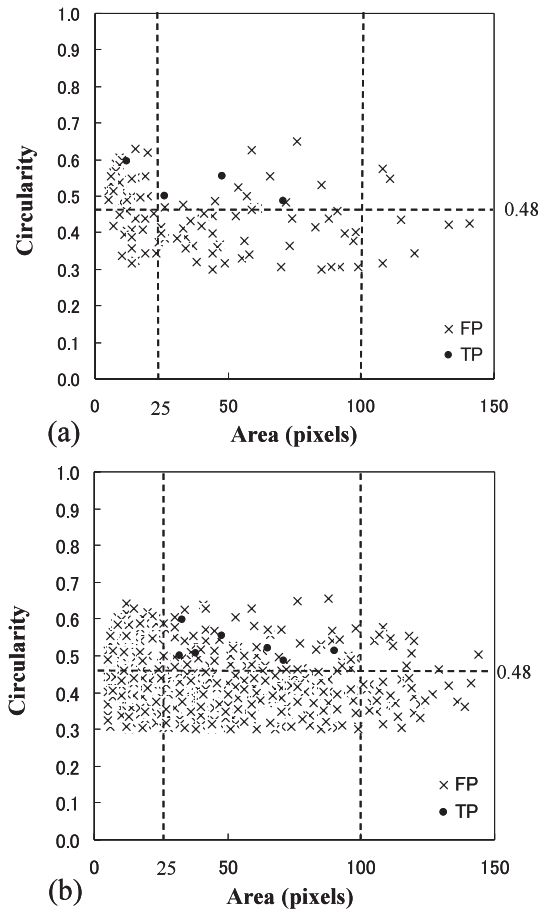

Fig. 8 Relationship between area and circularity after region growing, which were obtained from images with lacunar infarcts adjacent to the hyperintensive structures. (a) Training data (20 cases). (b) Testing data (80 cases). The dotted lines indicate the thresholds for eliminating FPs.

infarct with a high-intensity signal in a T2-weighted image should have a relatively lower intensity when compared to its surrounding area in the corresponding position on a T1-weighted image. On the contrary, FPs do not show such variations in T1- and T2-weighted images. In addition, many FPs detected from T2-weighted images were a part of the cerebral sulci or cerebrum. To eliminate such FPs, the cerebral parenchyma region was extracted, and the candidates who showed regions outside this region were considered as FPs. This method enables the elimination of most FPs along the cerebral parenchyma without losing most TPs. Moreover, one of the important reasons for using T1-weighted images is to avoid misclassification of hemorrhages as lacunar infarcts because the former also shows high intensities in both T1- and T2-weighted images. This processing is explained below in detail. Figure 9 illustrates the flowchart for eliminating the FPs by using T1-weighted images.

(a) Preprocessing: The median filter (3×3) was applied to the T1-weighted image in order to reduce noise.

(b) Extraction of the cerebral parenchyma: The gray-level histogram is calculated by considering all the pixels of

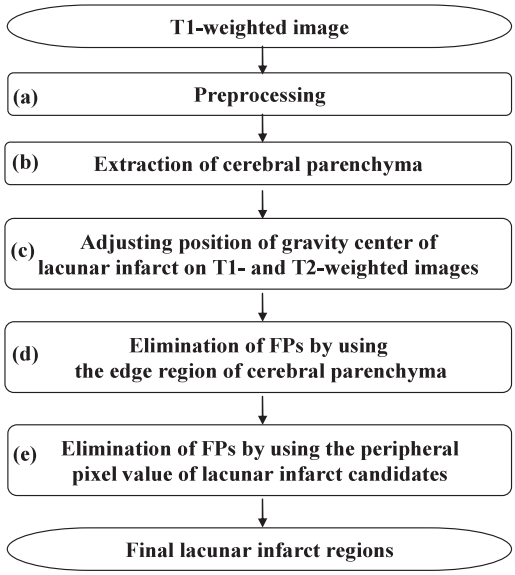

Fig. 9 Flowchart for eliminating FPs by using a T1-weighted image (Part B).

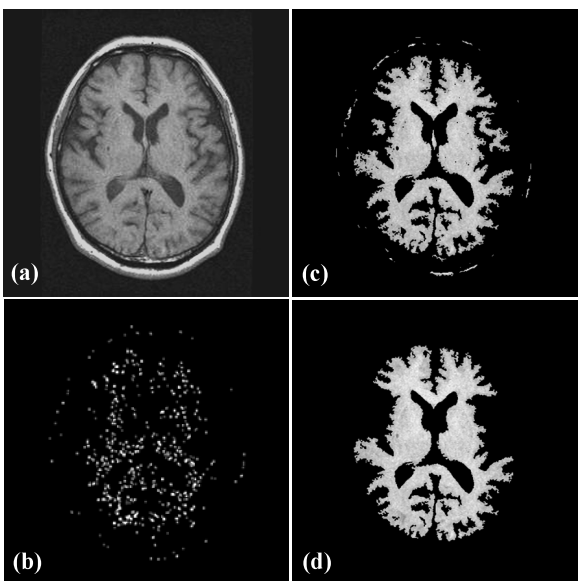

Fig. 10 Examples of extraction of cerebral parenchyma. (a) T1-weighted image. (b) Seed points for region growing. (c) The resulting image after region growing. (d) Extracted cerebral parenchyma regions.

the preprocessed image. The pixels of the brightest peak in the histogram are set as the seed points of region growing. The cerebral parenchyma region is extracted by using features such as size and circularity. The histogram obtained from T1-wighted images includes cerebral parenchyma regions, background, and other tissues. Thus, it is difficult to extract the cerebral parenchyma region by using a fixed threshold value obtained with other sophisticated methods like those employed by Otsu [20] or Kittler [21]. In this study, we used a method based on region growing. Figure 10 illustrates examples of extraction of cerebral parenchyma. Two large areas are not detected in Fig. 10 by using this method. However, lacunar infarcts are not detected in these

undetected regions because the occlusion of a penetration brain artery in the deep white matter is the cause of lacunar infarcts, and thus lacunar infarcts are detected around the basal ganglia.

(c) Adjusting the position of the gravity center of lacunar infarct in T1- and T2-weighted images: A typical lacunar infarct region in a T2-weighted image has a higher contrast as compared to that of the surrounding area and is marked as a high-intensity signal region. This is because the empty holes (lacunae) are filled with CSF in the center and have gliosis at the periphery [22], [23]. Although the lacunar infarct region appears as a low-intensity area in a T1-weighted image, its size usually appears smaller when compared to that observed in a T2-weighted image; moreover, the shape of the region also differs. This is an important reason why a lacunar infarct region with surrounding gliosis can only be observed in a T2-weighted image, but is not visible in a T1-weighted image. Consequently, the positions of the gravity centers in T2- and T1-weighted images differ, and this makes it impossible to use the gravity centers in T2- and T1-weighted images without any adjustments.

First, a region of interest (ROI) of a relatively larger size (13 × 13 pixels) was selected from the T1-weighted image using the gravity center of a lacunar infarct candidate detected in the T2-weighted image as the center of the ROI. Next, the small-sized ROIs (3×3 pixels) were scanned within the large-sized ROI in one pixel steps, and the sum of the gray values in each small ROI was calculated. The center coordinate of ROI with a minimum sum was selected from the total number of ROIs (11 × 11 pixels) as a new gravity center candidate (T1 process). Finally, in order to verify this gravity center, the mean pixel values of a 3 × 3 pixel ROI in the T2-weighted image were compared with the corresponding gravity centers of the T1 process. If the mean pixel value of this ROI obtained by the T1 process was greater than that obtained by the T2 process, the final gravity center in the T1-weighted image was decided; otherwise, this 3 × 3 pixel ROI was discarded and the next ROI was considered. This procedure was repeated until the ROI that satisfied this detection condition was located.

(d) Elimination of FPs by using the region at the edge of the cerebral parenchyma: Most of the FPs detected in the T2-weighted image were located in the cerebral sulci or a part of the cerebral ventricle. By using the information on the positions of the cerebral parenchyma derived from (a) in the T1-weighted image, FPs in the cerebral sulci that were mainly present at the edge of the cerebral parenchyma were eliminated.

(e) Elimination of FPs by using the peripheral pixel value of the lacunar infarct candidates: Neuroradiologists and/or neurosurgeons often focus on the contrast between the target and its peripheral region while inspecting an ROI or giving their opinion about a lesion from these images. Similarly, during the inspection of the images of the lacunar infarct candidate, the relative contrast between a candidate and its peripheral region is considered as an important parameter for identifying the lesion from the background.

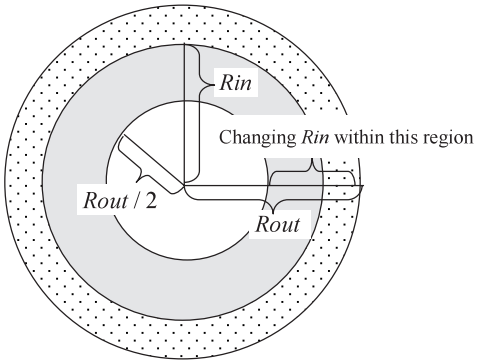

Fig. 11 The method of calculating the peripheral gray value difference. R_{out} is the peripheral radius of the circle. R_{in} is the internal radius of the circle.

Our proposed method, referred to as the multi-circular regions difference method (MCRDM), also differentiates the candidates by comparing the mean pixel values in the lacunar infarct and peripheral regions of a T1-weighted image. Furthermore, it considers the area and gravity center features. The detailed method is explained in a stepwise manner below. Figure 11 illustrates the method of calculating the peripheral gray value difference. The final lacunar infarct was detected by calculating the difference in the pixel value of the candidate and the peripheral region.

Step 1: From the detected candidates of lacunar infarct in the T2-weighted image, the peripheral radius of the circle (R_{out}) was determined on the basis of the area of a candidate (S).

$$R_{out} = \sqrt{S/\pi} \tag{8}$$

Step 2: The internal radius of the circle (R_{in}) was altered within a range of $R_{out}/2 < R_{in} < R_{out}$. If $R_{in} < 2$, then discontinue the process.

1) The mean pixel value (*ave_in*) of the solid region within the circle of radius R_{in} in Fig. 11 was calculated.

2) The mean pixel value (*ave_out*) of the subtraction region, which is the dotted region shown in Fig. 11, between the circles of radii R_{out} and R_{in} was calculated.

3) The gray value difference of the two circles was calculated as follows:

$$\text{gray value difference} = (ave\_out) - (ave\_in) \tag{9}$$

4) If the maximum gray value difference < calculated gray value difference, then the calculated gray value difference = gray value difference

Step 3: The procedure described in Step 2 was repeated by increasing the circle radius by one pixel at a time until the radius was $R_{out} + 6$.

Step 4: From among the seven circles, the one that had the maximum gray value difference was selected as the ROI.

Step 5: If the gray value difference of the ROI was greater than 10.6, the candidate was considered as a TP for lacunar infarct.

The circle radius was set from R_{out} to $R_{out} + 6$ in Step 3

because the peripheral radius of the circle (R_{out}) was determined on the largest binary area of a candidate that was extracted by the MPB method based on the T2-weighted image and not the T1-weighted image. Since the shape and size of the lacunar infarct that appeared in the T1-weighted image was different from those of the lacunar infarct that appeared in the T2-weighted image, it was necessary to make a changeable region to be able to correctly investigate the peripheral pixels around the extracted lacunar infarct region in the T1-weighted image. The threshold value of the area was between 19 and 200 pixels or 2 to 8 pixels when expressed in radius. Therefore, the difference of 6 pixels in the radius can include lacunar infarcts of all sizes. These threshold values for the gray value difference of the ROI in Step 5 were determined empirically based on the distribution of the lacunar infarcts in the training dataset.

3. Experimental Results

3.1 Performance for Detection of Lacunar Infarcts

A total of 832 slices including both their T2- and T1-weighted images obtained from 100 cases (male: 54 and female: 46; average age: 61.1 years) without any history of occlusion or neurological findings were selected for our experiment. The selection of MR slices was limited to the cerebral region. The first slice was selected when basal ganglia appeared on the image. Other slices were then orderly selected toward the direction of the top of the head until the cerebral parenchyma region clearly disappeared from the cerebral ventricle region.

This database includes 12 normal cases without lacunar infarct and 88 abnormal cases with more than one lacunar infarct. The 295 images included 635 small lacunar infarcts, which were confirmed by a neuroradiologist and a neurosurgeon, and the other 537 images were normal slices.

In our experiment, 20 cases were selected randomly from a total of 100 cases to determine the optimized threshold values, and the remaining 80 cases were used to test the performance of our method.

In the training dataset comprising 20 cases, 159 slices including both the T2- and T1-weighted images (male, 12 and female, 8; average age, 66 years) without any history of occlusion or neurological findings were selected. These included 184 lacunar infarcts from 69 images, and in the remaining 90 images, no infarcts were observed. In the remaining 80 cases, 673 slices including both their T2- and T1-weighted images (male: 42 and female: 38; average age: 60 years) showed 455 lacunar infarcts in 226 images and no infarcts were observed in the remaining 447 images.

After optimizing the threshold values in 20 training cases, the performance of detecting the lacunar infarct regions was calculated. The overall performance of our method was as follows. In the training dataset of 20 cases, the sensitivity was 92.4% with 1.4 FPs per image, and specificity was 34.4%. The positive and negative predictive values were 58.5% and 81.9%, respectively. On the other hand, in the testing dataset of 80 cases, the sensitivity was 90.1% with 1.7 FPs per image and specificity was 30.0%. The positive and negative predictive values were 56.3% and 76.9%, respectively.

3.2 Examples of the Detected Lacunar Infarcts and FPs

Three images indicating the TPs and typical FPs are shown in Fig. 12. The detected TP adjacent to the lateral ventricle is indicated by a circle in Fig. 12 (a). This lacunar infarct region adjacent to the hyperintensive structures that were extracted successfully by using the morphological opening processing is described in Sect. 2.3.2 (a). Although almost region of this lacunar infarct was connected to the cerebral ventricle, it could be detected correctly by using a difference image with two circular kernels of different sizes.

The FPs indicated by a half-box located at the periventricular high-signal region (Fig. 12 (b)) and the frontal area of the cerebral ventricle (Fig. 12 (c)) were incorrectly detected as lacunar infarcts. The threshold values of size and shape of the lesions in the periventricular high-signal regions were in the range of those of the TPs of lacunar infarct; this possibly resulted in the incorrect detection (Fig. 12 (b)). This can be prevented by applying other effective methods like region growing that consider the positional relation of the lesion to the cerebral ventricle region. Moreover, the FPs in Fig. 12 (c) may be eliminated by applying the property of symmetry of cerebral ventricle wherein the changes in the right and left sides can be compared.

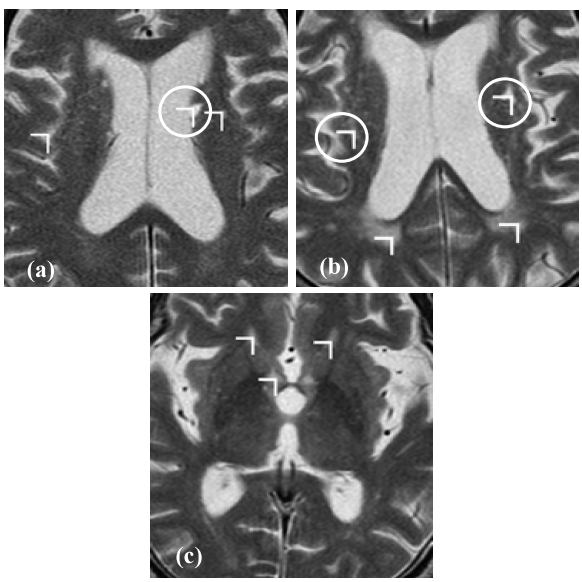

Fig. 12 Three images showing TPs and FPs. The circles indicate lacunar infarct regions. The half-boxes indicate the result of our detection. (a) The correctly detected TP adjacent to the lateral ventricle. (b) Two correctly detected TPs and two FPs (PVH: periventricular high-signal region) in the posterior horn of the lateral ventricle. (c) Three FPs in the frontal horn of the lateral ventricle.

4. Discussions

4.1 Effectiveness of Our Method for Eliminating FPs

Before the elimination of FPs in T1-weighted images, the total number of FPs was 3468 after the detection in T2-weighted images, an average of 5.2 (3468/673) FPs per image. There were 4 types of FPs: edge of cerebral parenchyma (ECP), periventricular high-signal region (PVH), cerebral ventricle or cistern (CV), and enlarged perivascular space (PVS), as illustrated in Table 1. The total number of FPs after their elimination in T1-weighted images was 1115. Their elimination rate from the ECP was 80%; periventricular high-intensity region, 19%; cerebral ventricle or cistern, 31.3%; and enlarged perivascular space, 0%. The result showed that our elimination method was most effective in the case of ECP with an approximate elimination rate of 80%.

Table 1 The effect of elimination process by using T1-weighted image (Part B in Fig. 1). ECP: edge of cerebral parenchyma. PVH: periventricular high-signal region. CV: cerebral ventricle or cistern. PVS: enlarged perivascular space.

Elimination of FPs \ Types of FPs		ECP	PVH	CV	PVS	Total
Before	Number	2722	352	348	46	3468
	Percentage	78.5	10.1	10.0	1.3	
After	Number	545	285	239	46	1115
	Percentage	48.9	25.6	21.4	4.1	

4.2 Possibility of Further Reduction in FPs

We have developed an algorithm for detecting the lacunar infarct region on MR images. Our proposed method has the advantage of reducing the number of FPs while maintaining a high TP rate. One of the important points to be noted is that the method of eliminating FPs along the edge of cerebral parenchyma, as described in Sect. 2.4 (d), effectively reduces the number of FPs without missing any TPs, and the FP elimination method described in Sect. 2.4 (e) misses only 4 true lacunar infarct regions. However, the regions with high-intensity pixels on the T2-weighted image, such as the enlarged perivascular space (PVS) and periventricular high-signal region (PVH), should be distinguished from lacunar infarct. The characteristics of enlarged perivascular space on an image, as described in [3], [4], and [22], were as follows: less than 3 mm in size, circular shape, salient boundary, no changes in the surrounding, smooth edges, symmetric, and located in the lower one-third part of the basal ganglia. Our method considered the size and position of enlarged perivascular space to distinguish it from a lacunar infarct region. However, this procedure was rather difficult to perform; even specialists had dissimilar views. According to Koto [22], the overlapping of the sizes of an enlarged perivascular space and a lacunar infarct is generally observed during clinical interpretation. The size of an enlarged perivascular space may reach 5–6 mm in some cases, making it difficult to distinguish them only on the basis of their size. However, it was possible to separate them considering their position and shape on the MR image.

Although the states of the periventricular high-signal region were elucidated at these states, many points remain unclear [23]. According to its definition, the periventricular high-signal region is included neither in the ischemic cerebral lesion nor in the lacunar infarct. Kobayashi et al. [4] divided the periventricular high-signal region into five phases from degree 0 to 4. Using their method, it was possible to differentiate the FPs of 3 to 10 mm in size in the periventricular high-signal region in the initial phase of degree 1, provided they are present in the MR slices. However, using our current method, it was difficult to extract the lacunar infarct region from the periventricular high-signal region whose size was less than 10 mm.

One of the possible features that enable us to distinguish these two regions was the size of the candidate in T1- and T2-weighted images. As mentioned in Sect. 2.4 (c), the typical lacunar infarct region in the T2-weighted image showed a high intensity region because the empty holes (lacunae) were filled with CSF in the center and had gliosis at the periphery [24]. However, the lacunar infarct region appeared as low intensity in the T1-weighted image, and it had a smaller size and showed a different shape when compared with those in the T2-weighted image. This was because a lacunar infarct region with surrounding gliosis was visible on the T2-weighted image, but was not visible in the T1-weighted image. Since no gliosis was observed in the periventricular high-signal region, the obvious difference could not be detected in T1- and T2-weighted images. Therefore, the difficulty in the differentiation of lacunar infarct in the periventricular high-signal regions can be overcome by comparing the size of the candidate in the two images.

At this stage, our MPB method used only the gravity center as the criteria for the differentiation of lacunar infarct from among all the detected candidates by multi-phase threshold values. To improve the detection accuracy and efficiency, new features have to be introduced. The change in the area and circularity features was now being considered useful. It was not possible for an isolated lacunar infarct candidate to connect with other components after the MPB processing. Therefore, the change in its area will not be rapid and would be at a consistent rate. Circularity was almost the same if the candidate was not connected to other regions. On the other hand, the rate of change in area and circularity of the binary images would rapidly increase in the case of lacunar infarcts connected with other high-intensity regions while the threshold values were changed. Therefore, it was possible to avoid FPs when detecting TPs by considering these change in rates.

4.3 Possibility of the Use of a FLAIR Image

The lacunar infarct regions can be clearly described by other imaging techniques besides the fast spin-echo T1- and T2-weighted images used in this experiment. For example, in fluid attenuated inversion recovery (FLAIR) sequences, we were able to detect lacunar infarctions by suppressing the signal intensity of the CSF by exclusively using the difference in T2-relaxation time between the CSF and the areas of infarction. Moreover, a proton density image can also detect the lacunar infarct.

The typical characteristic of lacunar infarct derived from these two different imaging techniques showed different findings when compared to those from T1- and T2-weighted images; the intensity in the center of lacunar infarct was higher than that in the peripheral gliosis region. Accordingly, the lacunar infarct region could be identified based on the features of the existing high-intensity gliosis region and the variation in contrast difference toward the center. In general, TP candidates could be identified as a high-intensity signal in a T2-weighted image, low-intensity signal in a T1-weighted image, and a higher signal intensity in the center than in the periphery of FLAIR or proton density images.

4.4 Possibility of the Use of 3D Information

Many FPs detected in Sect. 2.3.1 (the detection of the isolated lacunar infarct regions) belonged to a part of the cerebral sulci filled with CSFs; these appeared as isolated objects with high-intensity signals on the T2-weighted image. In order to eliminate these FPs, we can use the information from the images of the upper and lower slices at the same position of a candidate and study them in a 3-D view. Other FPs such as those in the anterior or posterior corners of the lateral cerebral ventricle were often detected as a pair of candidates, and these can be eliminated by using the symmetry of the brain as in the case of the periventricular high-intensity signal region.

5. Conclusions

This paper proposed an automatic method to detect the candidates of the lacunar infarct region in T2-weighted images and to eliminate FPs by using T1-weighted images. In the detection process using T2-weighted images, we proposed two detection procedures based on the multiple-phase binarization (MPB) method and morphological opening method. The final detection accuracy could be improved to a high TP rate of 90%. T1-weighted images were used to eliminate FP findings by targeting the region along the edge of the cerebral parenchyma and the peripheral pixel value of the lacunar infarct candidate. As a result, 68% of the total FPs detected from T2-weighted images were eliminated by the above two methods. In future experiments, we will include more cases for improving the detection accuracy and reducing the number of FPs detected from T2-weighted images by including features besides those used in our current scheme.

Acknowledgments

The authors thank Mr. A. Matsui and other members of Fujita Laboratory at Gifu University for their collaboration. This research was supported in part by a research grant from the Collaborative Center for Academy/Industry/Government of Gifu University; in part by a grant for the "Knowledge Cluster Creation Project" from the Ministry of Education, Culture, Sports, Science and Technology; and in part by the Ministry of Education, Culture, Sports, Science and Technology under a Grant-In-Aid for Scientific Research, Japanese Government.

References

[1] Y. Shinohara, "Significance and the present conditions of brain detection survey (Brain Doc)," The Journal of the Japanese Society of Internal Medicine, vol.86, pp.787–791, 1997.
[2] C.M. Fisher, "Lacunes: Small, deep cerebral infarcts," Neurology, vol.15, pp.774–784, 1965.
[3] T. Sawada, "What is the asymptopmatic brain vessel disease—The definition and diagnosis basis," The Journal of the Japanese Society of Internal Medicine, vol.86, pp.725–732, 1997.
[4] S. Kobayashi, "MRI and health screening of the brain: Asymptomatic cerebral infarction," Japanese Journal of Diagnostic Imaging, vol.17, no.2, pp.159–167, 1998.
[5] S. Kobayashi, H. Koide, and H. Bokura, "Prospective study on stroke onset in silent cerebral infarction," J. Stroke and Cerebrovascular Diseases, vol.6, pp.100–105, 1996.
[6] H. Kou, H. Suzuki, and J. Toriwaki, "Automated segmentation of MRI head images by 3-D region growing method which utilizes edge information," Transactions of the Japanese Society for Medical and Biological Engineering, vol.29, no.3, pp.170–177, 1991.
[7] N. Hayashi, S. Sanada, M. Suzuki, and Y. Matsuura, "Segmentation method of the cerebellum and brainstem on MR images using mathematical morphology," Medical Imaging and Information Sciences, vol.21, no.1, pp.109–115, 2004.
[8] K. Van Leemput, F. Maes, D. Vandermeulen, and P. Suetens, "Automated model-based tissue classification of MR images of the brain," IEEE Trans. Med. Imaging, vol.18, no.10, pp.897–908, 1999.
[9] I. Uwano, K. Fujiwara, K. Matsuda, M. Kameda, A. Doi, T. Inoue, and A. Ogawa, "An extraction of a brain tumor area from MRI images using 3D region growing," IEICE Technical Report, MI2002-73, 2002.
[10] D.L. Wilson and J.A. Nobel, "Segmentation of cerebral vessels and aneurysms from MR angiography data," Lect. Notes Comput. Sci., vol.1230, pp.423–428, 1997.
[11] D.L. Wilson and J.A. Nobel, "An adaptive segmentation algorithm for time-of-flight MRA data," IEEE Trans. Med. Imaging, vol.18, no.10, pp.938–945, 1999.
[12] H. Arimura, Q. Li, Y. Korogi, T. Hirai, H. Abe, Y. Yamashita, S. Katsuragawa, R. Ikeda, and K. Doi, "Automated computerized scheme for detection of unruptured intracranial aneurysms in three-dimensional MRA," Acad. Radiol., vol.11, pp.1093–1104, 2004.
[13] T. Hirai, Y. Korogi, H. Arimura, S. Katsuragawa, M. Kitajima, M. Yamura, Y. Yamashita, and K. Doi, "Intracranial aneurysms at MR angiography: Effect of computer-aided diagnosis on radiologists' detection performance," Radiology, vol.237, pp.605–610, 2005.
[14] Y. Uchiyama, H. Ando, R. Yokoyama, T. Hara, H. Fujita, and T.

Iwama, "Computer-aided diagnosis scheme for detection of unruptured intracranial aneurysms in MR angiography," Proc. 2005 IEEE Engineering in Medicine and Biology 27th Annual Conference, paper #296, 2005.

[15] H. Arimura, Q. Li, Y. Korogi, T. Hirai, S. Katsuragawa, Y. Yamoshita, K. Tsuchida, and K. Doi, "Computerized detection of intracranial aneurysms for three-dimensional MR angiography: Feature extraction of small protrusions bases on a shape-based difference image technique," Med. Phys., vol.33, no.2, pp.394–401, 2006.

[16] N. Hayashi, Y. Matsutani, T. Matsumoto, H. Mori, A. Kunimatsu, O. Abe, S. Aoki, K. Ohtomo, N. Takano, and K. Matsumoto, "Feasibility of a curvature-based enhanced display system for detecting cerebral aneurysms in MR angiography," Magnetic Resonance in Medical Scienece, vol.2, pp.29–36, 2003.

[17] S. Kobayashi, K. Kondo, and Y. Hata, "Computer-aided diagnosis of intracranial aneurysms in MRA images with case-based resoning," IEICE Trans. Inf. & Syst., vol.E89-D, no.1, pp.340–350, Jan. 2006.

[18] R. Yokoyama, Y. Lee, T. Hara, H. Fujita, T. Asano, H. Hoshi, T. Iwama, and N. Sakai, "An automated detection of lacunar infarct regions in brain MR images: Preliminary study," Japanese Journal of Radiological Technology, vol.50, no.3, pp.399–405, 2002.

[19] T. Araki, ed., A Key to MRI Interpretation, pp.40–41, Shujunsha, Tokyo, 1995.

[20] N. Otsu, "Discriminant and least square threshold selection," Proc. 4IJCPR, pp.592–596, 1978.

[21] J. Kittler and J. Illingworth, "On threshold selection using clustering criteria," IEEE Trans. Syst. Man Cybern., vol.15, no.5, pp.652–655, 1985.

[22] A. Koto, Y. Hashimoto, H. Tougi, and Y. Fukuuchi, Brain and Circulation, vol.6, no.2, pp.11–23, 2001.

[23] W.T. Longstreth Jr, T.A. Manolio, and A. Arnold, "Clinical correlates of white matter findings on cranial magnetic resonance imaging of 3301 elderly: The cardiovascular health study," Stroke, vol.27, pp.1274–1282, 1996.

[24] A. Nagazumi, M. Takahashi, and Y. Ktayama, "Medical treatment of silent lacuna stroke," Brain and Circulation, vol.6, no.2, pp.39–40, 2001.

Ryujiro Yokoyama received the B.S. and M.S. degrees in Electrical Engineering from Gifu University, Japan, in 2000 and 2002, respectively. Currently, he is a Ph.D. candidate in the Department of Intelligent Image Information, Graduate School of Medicine, Gifu University, Japan. He is also a radiological technologist and working in Gifu University Hospital from 1976 till now. His research interests include medical image processing and pattern recognition.

Xuejun Zhang received the B.S. degree in Physics from Guangxi University, P.R.China, in 1991, and the M.S. degree in Electronics and Information Systems Engineering from Gifu University, Japan, in 2001. Currently, he is a Ph.D. candidate in Graduate School of Engineering, Gifu University, Japan. His research interests include artificial neural network, digital image processing and pattern recognition.

Yoshikazu Uchiyama received the M.S. and Ph.D. degrees in Computer Science and Systems Engineering from Miyazaki University, Japan, 1997 and 2000, respectively. He is currently a visiting associate professor in the Department of Intelligent Image Information, Graduate School of Medicine, Gifu University, Japan. His research interests include image processing, pattern recognition, computer-aided diagnosis.

Hiroshi Fujita received the B.S. and M.S. degrees in Electrical Engineering from Gifu University, Japan, in 1976 and 1978, respectively, and Ph.D. degree from Nagoya University in 1983. He was a Research Associate at University of Chicago, USA, from 1983 to 1986. He is currently a Professor in the Department of Intelligent Image Information, Graduate School of Medicine, Gifu University, Japan. His research interests include computer-aided diagnosis system, image analysis and processing, and image evaluation in medicine.

Takeshi Hara received the M.S. and Ph.D. degrees in Electrical Engineering from Gifu University, Japan, in 1995 and 2000, respectively. He is currently a associate professor in the Department of Intelligent Image Information, Graduate School of Medicine, Gifu University, Japan. His research interests include computer network, medical image processing and pattern recognition.

Xiangrong Zhou received the M.S. and Ph.D. degrees in information engineering from Nagoya University, Japan in 1997 and 2000 respectively. From 2000 to 2002, he continued his research in medical image processing as a postdoctoral researcher at Gifu University, and currently, he is a research associate of graduate school of medicine, Gifu University, Japan.

Masayuki Kanematsu M.D. received the Ph.D. degree at Gifu University in 1995. He served as a visiting scholar at Dept. of Radiology, University of Pittsburgh from 1994 to 1995. He has been appointed to the associated professorship of Radiology Services at Gifu University Hospital since 2001. He was invited as a visiting full professor of Dept. of Radiology, University of North Carolina from 2002 to 2003.

Takahiko Asano M.D. He graduated from Gifu University School of Medicine in 1997, and has been appointed as an assistant professor of Gifu University Hospital since 1998. He has been certified as a board radiologist of Japan Radiological Society since 2003. His research interests include neuroradiology and nuclear medicine.

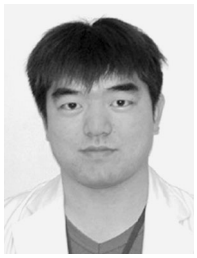

Hiroshi Kondo M.D. He graduated from Gifu University School of Medicine in 1997. He is the Chief Radiologist of Department of Radiology, Kizawa Memorial Hospital, Minokamo, Japan. His specialty is abdominal radiology and interventions. He was awarded for his achievement in clinical radiologic research in 2002 by the Alumni Association of Gifu University School of Medicine.

Satoshi Goshima M.D., Ph.D. He graduated from Shimane Medical University in 2000, and has been appointed as an assistant professor of Gifu University Hospital since 2006. He has been certified as a board radiologist of Japan Radiological Society since 2005. He obtained a degree of medicine at Gifu University in 2006. His research interests include abdominal radiology and interventional radiology.

Hiroaki Hoshi M.D. received the Ph.D. degree at Miyazaki Medical School in 1987. He served as a visiting scholar at the Montreal Neurological Institute from 1991 to 1992. He has been appointed to the chairmanship of Department of Radiology at Gifu University School of Medicine since 1995.

Toru Iwama M.D. received the Ph.D. degree at Gifu University Graduate School of Medicine in 1990. He has been appointed to the chairmanship of Department of Neurosurgery at Gifu University Graduate School of Medicine since 2004. His major fields are cerebrovascular surgery and benign brain tumor surgery.